Electrochemistry Communications 176 (2025) 107929

Contents lists available at ScienceDirect

Electrochemistry Communications

journal homepage: www.elsevier.com/locate/elecom

A simple and effective catalyst recovery protocol for H_2-PEMFCs

Marc Ayoub [a,b], Rohit Rajendran Menon [a,b], Simon Thiele [a,b], Matthew Brodt [a,*]

[a] Helmholtz-Institute Erlangen-Nürnberg for Renewable Energy (IET-2), Forschungszentrum Jülich, Cauerstr. 1, 91058 Erlangen, Germany
[b] Department of Chemical and Biological Engineering, Friedrich-Alexander-Universität Erlangen-Nürnberg, Cauerstr. 1, 91058 Erlangen, Germany

ARTICLE INFO

Keywords:
Fuel cells
Durability
Recovery
Degradation

ABSTRACT

Catalyst degradation in the cathode electrode for H_2-PEM (hydrogen proton-exchange membrane) fuel cells is a crucial topic to tackle to achieve high durability and efficiency. Despite ongoing research, a concurrently fast, easy-to-adapt, and effective recovery protocol is still missing. In this study, we report a fast and easy-to-adapt recovery protocol that significantly mitigates the negative effects associated with catalyst degradation for the cathode electrode in H_2-PEMFCs. Following accelerated stress tests (AST) of 30,000-cycles, membrane-electrode assemblies (MEAs) using our new recovery protocol exhibit remarkable higher end-of-life performance compared to similar MEAs subjected to the same AST but utilizing the DOE-defined recovery protocol. The end-of-life differences for the new recovery protocol are over 100 % increase in power density at 0.6 V and around 26 % increase at peak power density. By analyzing performance, the Tafel slope, the electrochemical surface area (ECSA), and impedance data, the improvements are traced back to better catalyst recovery and thus improved performance at end-of-life.

1. Introduction

A key technology for the transition towards an environmentally friendly energy cycle is the H_2-PEMFC, where O_2 from air electrochemically reacts with H_2 to produce water with usable electric and thermal energy. The DOE and the FCH Joint Undertaking (now Clean Hydrogen Partnership) have published targets and milestones for a successful commercialization of PEMFCs [1,2]. Among the goals is the need to reduce the overall costs by utilizing less of the expensive platinum (Pt) catalyst in the cathode electrode while at the same time maintaining high performance, durability, and lifetime [1,2]. However, multiple studies have shown that utilizing low Pt loadings is linked with increased challenges related to durability [3–5]. Pt dissolution, poisoning, Ostwald ripening, and the formation of Pt oxides are among the degradation processes that result in significant potential losses at low loadings [3,5–7]. The oxide formation processes on the Pt surface are thermodynamically favorable at high potentials $\gtrapprox$ 0.7 V [6,8]. Upon oxidation, 2D and 3D layers of oxides can form on Pt, which can hinder the oxygen reduction reaction (ORR) [6,9,10]. Furthermore, ionomer restructuring during operation (e.g., adsorption of sulfates/sulfonates) can block active sites and hinder the ORR [11,12].

Many researchers have focused on finding alternative materials and designs for the cathode catalyst to tackle these challenges. Specifically, researchers are investigating alloy catalysts such as Pt-Co, alternative catalyst support structures such as carbon nanoshells, and Pt-free alternatives [7,13]. Few researchers have looked into different methods for recovering Pt catalyst activity after degradation. Among them, one recovering method employs cyclic voltammetry (CV) between 0 and 100 mV with scan rates of 10–50 $mV{\cdot}s^{-1}$, with H_2 on the anode and nitrogen (N_2) on the cathode [10]. In another protocol, the cell is cooled to 40 °C, while the relative humidity (RH) for H_2 and air are increased to 100 % RH, and a reducing potential of 0.3 V is applied at 150 kPa for 2 h [14]. Another protocol reduced the catalyst by purging the cathode with $H_{2(g)}$ and/or by performing cathodic H_2 pumping feeding fully saturated $H_{2(g)}$ to the cathode [15]. Generally, cathodic catalyst reactivation requires reductive conditions, which is generally agreed to be $\lessapprox$ 0.4 V vs SHE for Pt oxides [16,17]. Also, ionomer adsorption on the active catalyst can be recovered by operation under highly humidified conditions and reductive potentials [6,18]. At high RHs, proton conductivity and swelling increase, aiding reduction and desorption from the catalyst surface. With these in mind, we developed a novel protocol for Pt recovery after degradation. Compared to the other procedures, our protocol does not require changes of reactant gases and takes less time to execute. Considerable improvements are achieved compared to the standard DOE protocol.

* Corresponding author.
E-mail address: ma.brodt@fz-juelich.de (M. Brodt).

https://doi.org/10.1016/j.elecom.2025.107929
Received 19 November 2024; Received in revised form 9 March 2025; Accepted 7 April 2025
Available online 10 April 2025

2. Experimental

2.1. Ink preparation

A short-sided chain (SSC) 3 M™ ionomer with an equivalent weight (EW) of 800 g·mol^{-1} was used to prepare a 20 wt% dispersion. The solvent comprised 60 wt% anhydrous 1-propanol and 40 wt% Milli-Q water with a resistivity of 18.2 MΩ·cm. 1-propanol was first added to the ionomer in a 500 mL heat-suitable Schott bottle on a heating plate set at 80 °C and 500 RPM ($T_{internal} \approx 50$ °C). After swelling the ionomer for 2 h, the remaining 40 wt% of water was added, and the mixture was dispersed over three days, followed by a 1-day resting period.

A catalyst ink with 40 % Pt/C catalyst (TEC10V40E, Tanaka) having a solid weight content of 11 wt% was prepared as in our previous study [19]. The ionomer-to-carbon ratio of the ink was 0.80.

2.2. Electrode manufacturing

Doctor-blading at 60 °C with a wet-film thickness of 70 μm on decal sheets was done similarly to our previous study but here with a coating speed of 100 mm·s^{-1} [19]. The electrodes were annealed for 10 min at 180 °C as per manufacturer's recommendation. The dry film thickness is 4 μm measured with scanning electron microscopy. The catalyst loading is 0.103 ± 0.006 $mg_{Pt}·cm^{-2}$ for the cathodes and 0.104 ± 0.011 $mg_{Pt}·cm^{-2}$ for the anodes. The electrodes were then stamped into 25 cm^2 samples (5·5 cm^2) and hotpressed on 49 cm^2 (7·7 cm^2) GORE-SELECT® Membranes (M775.15, thickness 15.5 μm) with the same method and settings as before [19].

2.3. Electrochemical measurements

The catalyst-coated-membranes were assembled in a commercial 25 cm^2 Scribner cell fixture with triple-channel serpentine flow fields (graphitic), and 25 cm^2 gas diffusion layers (GDLs) were used (H14CX483, Freudenberg). Glass-fiber-reinforced PTFE gaskets (Fiberflon) were employed to compress the GDLs by 19 ± 1 %, and a 5 N·m torque was used for the cell. The membrane-electrode-assemblies (MEAs) were tested in a commercial 850 g fuel cell system (Scribner Associates Inc.) using a VMP-300 potentiostat (BioLogic).

Measurements started with a short test using linear sweep voltammetry (LSV) at 80 °C, atmospheric pressure, once at 150 kPa absolute, fully humidified conditions, 1.00 L·min^{-1} H_2 on the anode, 1.00 L·min^{-1} N_2 on the cathode, and a scan rate of 2 mV·s^{-1} from 0.10 V to 0.4 V [20,21].

Then, the cell was conditioned by voltage cycling 10 times between 0.6 V and 0.3 V, 20 min hold times at each step, and 2 min OCV in between [22]. The cell was at 150 kPa absolute, 80 °C, 1.00 L·min^{-1} of H_2 on the anode, 3.75 L·min^{-1} of synthetic air on the cathode, and 100 % RH. This resulted in steady-state conditions.

Polarization curve measurements were then conducted under the same conditions using galvanostatic steps with 10 steps from 0 to 0.150 A·cm^{-2} and then 11 steps further until 2.0 A·cm^{-2}. Each step was held for two minutes, of which the last 30 s were averaged to represent the polarization response. After the two minutes, galvanostatic impedance measurements were performed with 10 % amplitude from 200 kHz to 1 Hz with 10 points per decade and 3 averaged measurements per frequency.

For one sample, the protonic sheet resistance based on 3 measurements was quantified at beginning of life (BOL) at 0.2 V, 1.00 L·min^{-1} H_2 on the anode, 1.00 L·min^{-1} N_2 on the cathode, 100 % RH, 80 °C, and atmospheric pressure. An amplitude of 10 mV was used between 200 kHz and 200 mHz. The protonic sheet resistance was fitted with a transmission line model (TLM) using the EC-Lab software by means of the "Randomize+Simplex" method [23,24].

CV measurements were performed at 200, 350 and 500 mV·s^{-1} consecutively from 0.03 to 0.6 V at 80 °C, 100 % RH, atmospheric pressure, using 1.00 L·min^{-1} of 5 % H_2 and 95 % N_2 at the anode, and 0 L·min^{-1} at the cathode. ECSA calculations were made for 200 mV·s^{-1} by integration between 0.05 V and 0.40 V similar to before [19,25].

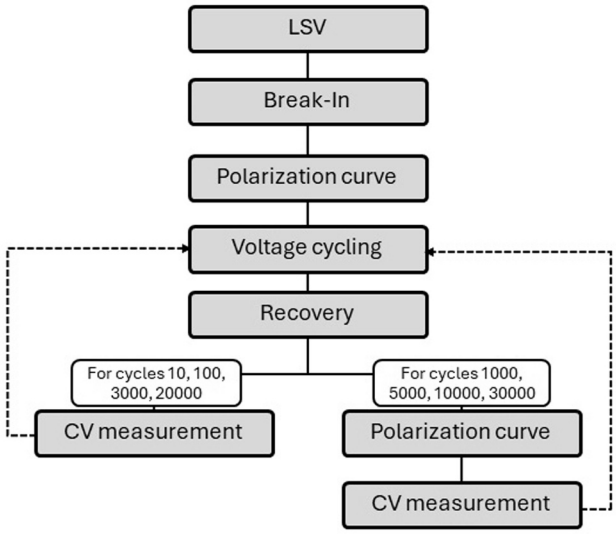

Fig. 1. Utilized AST protocol for this study.

Table 1
DOE defined recovery protocol at 80 °C, 100 % RH, and 150 kPa absolute pressure. The flow rates are in standard liter per minutes (SLPM).

Step	Step Name	Anode gas	Anode Flow (SLPM)	Cathode gas	Cathode Flow (SLPM)	Duration (s)
1	N_2 soak	100 % N_2	2	100 % N_2	4	120
2	Air soak	N/A	0	Air	4	900
3	N_2 soak	100 % N_2	2	100 % N_2	4	120
4	H_2 soak	100 % H_2	2	N/A	0	600
5	H_2-air back on	100 % H_2	2	Air	4	5

Table 2
Novel protocol described here: Differential pressure hydrogen pumping (dP_{HP}) recovery protocol at T_{cell} = 70 °C and $T_{humidifiers}$ = 80 °C.

T_{cell} (°C)	P_{anode} (kPa)	$P_{cathode}$ (kPa)	Anode Flow (SLPM)	Applied Voltage (V)	Cathode Flow (SLPM)	Duration (s)
70	250	210	1.8 H_2	−0.100	0	600

2.4. AST procedure

The Pt accelerated stress tests were performed according to the DOE protocol, Fig. 1, with the difference being the recovery procedure [1].

In Tables 1 and 2, the recovery protocols are provided. These are performed according to Fig. 1. For Tafel slope analysis, the polarization curves were corrected for the H_2-crossover, high-frequency resistance (HFR), and protonic sheet resistance resulting in the IR_{free} plot. The Tafel slope was calculated in the linear region until 0.100 A·cm^{-2}.

3. Results and discussion

The DOE recovery protocol (Table 1) includes series of steps over 29 min that only alter which gases, if any, are fed to each electrode: first N_2 on both electrodes, then only air on the cathode, then N_2 on both electrodes, then H_2 on the anode, and finally back to normal H_2/air operation. So, the DOE protocol is designed to condition the cathode to air for ORR and the anode to H_2 for HOR; it does not involve changes in voltage, pressure, or temperature. In contrast, in our protocol, referred to here as the differential pressure hydrogen pumping (dP_{HP}) protocol, a voltage and pressure differential is established between the two electrodes and the cell temperature is reduced, resulting in supersaturated conditions. H_2 fed to the anode is oxidized into protons and electrons. On the cathode side, the protons are reduced by electrons from the electric circuit to form H_2 gas, resulting in an anodic H_2 pumping mode. Hence, we increase the H_2 concentration on the cathode side. By applying higher pressure at the anode, the H_2 concentration at the cathode further increases.

$$\text{Anode}: \quad H_2 \rightarrow 2H^+ + 2e^- \tag{1}$$

$$\text{Cathode}: \quad 2H^+ + 2e^- \rightarrow H_2 \tag{2}$$

To confirm the effectiveness of the dP_{HP} protocol, three MEAs per recovery protocol were tested with the standard DOE accelerated stress test (AST) protocol for Pt dissolution. Fig. 2 shows the performances and HFRs at BOL until end of life (EOL).

At BOL (Fig. 2a) the performances are, as expected, the same since the ASTs and recovery had not started yet. Upon voltage cycling 1000 times and after the first recovery (Fig. 2b), a higher performance is visible for the samples with the dP_{HP} recovery protocol than the DOE. Also, the dP_{HP} peak power density (of 850 mW·cm^{-2}) achieved remains almost unchanged despite not reaching the 2.2 A·cm^{-2} as at BOL. After 5000 cycles (Fig. 2c), the visible differences in performance become more pronounced. However, compared to before, the dP_{HP} peak power density shows a drop compared to Fig. 2a and b. After 10,000 and 30,000 cycles (Fig. 2d and e), the differences become slightly more visible, with continuous peak performance decline. The HFRs throughout the AST protocols show no noticeable changes (Fig. 2f), indicating no significant membrane degradation. Table 3 summarizes the relative improvement in peak power density and at 0.6 V for the dP_{HP} protocol MEAs as compared with the DOE ones at various cycle numbers.

Table 4 and Fig. 3a show the average Tafel slopes at different cycles for the different recovery protocols. At BOL the Tafel slopes are approximately the same at 66–69 mV·dec^{-1}. However, after 5000 cycles, the Tafel slope for the DOE protocol is already above 80 mV·dec^{-1}, whereas for the dP_{HP} protocol, the Tafel slope remains below 80 mV·dec^{-1} after 10,000 cycles. At 30000 cycles, the DOE Tafel slope has an average value of 137 mV·dec^{-1}, compared with 95 mV·dec^{-1} for the dP_{HP} protocol, indicating better kinetic behavior for the MEAs after the dP_{HP} protocol.

Table 3
Relative increase in power density at peak power and at 0.6 V for the dP_{HP} recovery protocol as compared to the DOE recovery protocol. The deviation for peak power are min-max based, and the values at 0.6 V were extrapolated having hence no error bars.

Cycle number	1000	5000	10,000	30,000
↗ in peak power density (%)	6.2 ± 2.6	12.2 ± 4.2	16.9 ± 0.4	27.5 ± 6.7
↗ in power density at 0.6 V (%)	37	64	82	113

Table 4
Calculated Tafel slopes at different cycles for the different recovery protocols, with the values rounded to the nearest unit digit resulting in negligible error bars.

Cycle number	Tafel slope (mV·dec^{-1}), DOE	Tafel slope (mV·dec^{-1}), dP_{HP}
BOL	66	69
1000	72	71
5000	85	73
10,000	91	76
30,000	137	95

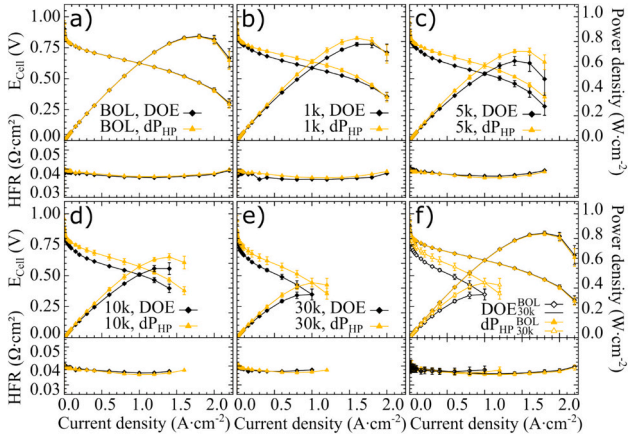

Fig. 2. Polarization curves and HFRs measured at 100 % RH, 150 kPa absolute, 1 L·min^{-1} H_2 anode, 3.75 L·min^{-1} air cathode at a) BOL, b) 1000 cycles, c) 5000 cycles, d) 10,000 cycles, e) 30,000 cycles. f) comparison between BOL and EOL. Error bars represent the standard deviation of 3 tested MEAs.

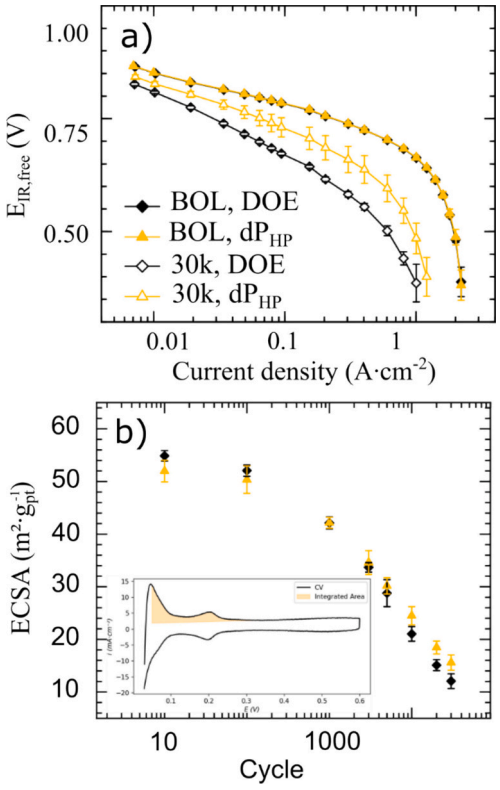

Fig. 3a. Comparison of the different protocols' Tafel slope at BOL and EOL. b) Change in ECSA after voltage cycling for the dP and DOE protocols. The inlaid CV shows the area used to calculate the ECSA. The error bars represent the min-max deviations for the measurements.

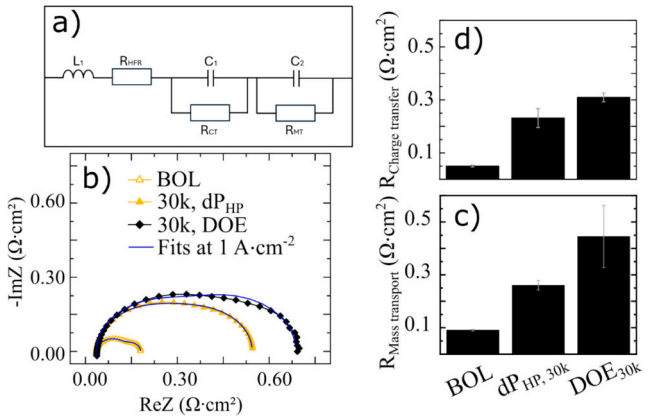

Fig. 4. a) Equivalent circuit with inductor, resistor, and 2 RC elements to fit impedance at 1 A·cm^{-2}.b) Representative fits at 1 A·cm^{-2} for the different protocols at BOL and EOL. c) Calculated charge transfer resistances. d) Calculated mass transport resistances. The error bars are based on min-max deviations.

Fig. 3b illustrates the change in ECSA for the different cycles. The dP_{HP} protocol seems to retain more active area after cycle 30,000. However, the overall difference is minimal and more distinguishable in the Tafel slope.

Impedance data at 1 A·cm^{-2} were fitted using a simple equivalent circuit to swiftly compare the losses for the different samples, Fig. 4 [12]. The dP_{HP} protocol is observed to result in lower charge transfer (R_{CT}) and mass transport resistances (R_{MT}) than the DOE protocol. A possible explanation is that the dP_{HP} recovery step, which resulted in high currents (> 2.2 A·cm^{-2}), also ensured a high water flux from anode to cathode (through diffusion, electro-osmotic drag, and Grotthuss and vehicular proton transport). These conditions could have restructured the ionomer and aided in the washing of adsorbed contaminants out while also reducing Pt oxides [6,11,12]. In contrast, the DOE recovery protocol lacks the same reducing conditions and water flux, resulting in lower recovery.

4. Conclusion

In this study, a recovery protocol for Pt degradation is presented, where a reductive potential is used to pump H_2 from the anode to the cathode. At the cathode, the H_2 with transported water can reduce formed Pt oxides while desorbing and washing contaminants out. A potential of −0.1 V was applied for 10 min with a differential pressure of 40 kPa. The applied potential, pressure, and recovery time are parameters that can be systematically varied in future experiments. Overall, this protocol is easy to implement and has relevance for FC systems, e.g. FC electric vehicles, where an additional or external power supply can be used to apply reductive currents.

CRediT authorship contribution statement

Marc Ayoub: Writing – original draft, Visualization, Methodology, Investigation, Data curation, Conceptualization. **Rohit Rajendran Menon:** Writing – review & editing, Methodology, Conceptualization. **Simon Thiele:** Writing – review & editing, Supervision, Funding acquisition, Conceptualization. **Matthew Brodt:** Writing – review & editing, Supervision, Methodology, Conceptualization.

Declaration of competing interest

The authors declare that they have no known competing financial interests or personal relationships that could have appeared to influence the work reported in this paper.

Acknowledgments

We express our gratitude to 3 M™ for providing the ionomer.

Data availability

Data will be made available on request.

References

[1] Energy.gov, *U.S. DRIVE, Fuel Cell Technical Team Roadmap*. Available. https://www.energy.gov/eere/vehicles/us-drive.
[2] Available. https://ec.europa.eu/research/participants/data/ ref/h2020/other/legal/jtis/fch-multi-workplan_en.pdf J.U. Governing Board, Fuel Cells and Hydrogen Joint Undertaking (FCH JU) Multi - Annual Work Plan, 2014–2020, 2014.
[3] G.P. Keeley, S. Cherevko, K.J.J. Mayrhofer, The stability challenge on the pathway to low and ultra-low platinum loading for oxygen reduction in fuel cells, ChemElectroChem 3 (1) (2016) 51–54, https://doi.org/10.1002/celc.201500425.
[4] P. Gazdzicki, J. Mitzel, A.M. Dreizler, M. Schulze, K.A. Friedrich, Impact of platinum loading on performance and degradation of polymer electrolyte fuel cell electrodes studied in a rainbow stack, Fuel Cells 18 (3) (2018) 270–278, https://doi.org/10.1002/fuce.201700099.
[5] R. Sgarbi, et al., Does the platinum-loading in proton-exchange membrane fuel cell cathodes influence the durability of the membrane-electrode assembly? Ind. Chem. Mater. 1 (4) (2023) 501–515, https://doi.org/10.1039/D3IM00059A.
[6] J. Mitzel, Q. Zhang, P. Gazdzicki, K.A. Friedrich, Review on mechanisms and recovery procedures for reversible performance losses in polymer electrolyte membrane fuel cells, J. Power Sources 488 (2021) 229375, https://doi.org/10.1016/j.jpowsour.2020.229375.
[7] H. Ma, Y. Tong, Y.M. Hung, X. Wang, Progress on the durability of catalyst layer interfaces in proton-exchange membrane fuel cells, Process. Saf. Environ. Prot. 192 (2024) 358–377, https://doi.org/10.1016/j.psep.2024.10.047.
[8] S.G. Rinaldo, W. Lee, J. Stumper, M. Eikerling, "Mechanistic principles of platinum oxide formation and reduction," (in en;en), Electrocatalysis 5 (3) (2014) 262–272, https://doi.org/10.1007/s12678-014-0189-y.
[9] M. Teliska, W.E. O'Grady, D.E. Ramaker, Determination of O and OH adsorption sites and coverage in situ on Pt electrodes from Pt L(2,3) X-ray absorption spectroscopy, J. Phys. Chem. B 109 (16) (2005) 8076–8084, https://doi.org/10.1021/jp0502003.
[10] H. Xu, R. Kunz, J.M. Fenton, Investigation of platinum oxidation in PEM fuel cells at various relative Humidities, Electrochem. Solid-State Lett. 10 (1) (2007) B1, https://doi.org/10.1149/1.2372230.
[11] Q. Zhang, M. Schulze, P. Gazdzicki, K.A. Friedrich, Comparison of different performance recovery procedures for polymer electrolyte membrane fuel cells, Appl. Energy 302 (2021) 117490, https://doi.org/10.1016/j.apenergy.2021.117490.
[12] Q. Zhang, M. Schulze, P. Gazdzicki, K.A. Friedrich, Temperature reduction as operando performance recovery procedure for polymer electrolyte membrane fuel cells, Energies 17 (4) (2024) 774, https://doi.org/10.3390/en17040774.
[13] M.M. Tellez-Cruz, J. Escorihuela, O. Solorza-Feria, V. Compañ, Proton exchange membrane fuel cells (PEMFCs): advances and challenges, Polymers 13 (18) (2021), https://doi.org/10.3390/polym13183064.
[14] J.P. Owejan, J.E. Owejan, W. Gu, Impact of platinum loading and catalyst layer structure on PEMFC performance, J. Electrochem. Soc. 160 (8) (2013) F824–F833, https://doi.org/10.1149/2.072308jes.
[15] H. Choo, D. Chun, J. Lee, H. Shin, et al., Performance Recovery of Fuel Cell Stack for FCEV, SAE Technical Paper (2015) 2015–01-1171, https://doi.org/10.4271/2015-01-1171.
[16] R. Sharma, K. Rode Nielsen, P. Brilner Lund, S. Bredmose Simonsen, L. Grahl-Madsen, S. Ma Andersen, Sustainable platinum recycling through electrochemical dissolution of platinum nanoparticles from fuel cell electrodes, ChemElectroChem 6 (17) (2019) 4471–4482, https://doi.org/10.1002/celc.201900846.
[17] F. Guillet, M. Chatenet, A. Paul, L. Svecova, L. Dubau, Electrochemical recovery of Pt/C electrocatalyst: optimization of the potential range on the leaching process and application to an aged MEA, Ind. Chem. Mater. 2 (1) (2024) 118–131, https://doi.org/10.1039/D3IM00085K.
[18] S. Jomori, K. Komatsubara, N. Nonoyama, M. Kato, T. Yoshida, An experimental study of the effects of operational history on activity changes in a PEMFC, J. Electrochem. Soc. 160 (9) (2013) F1067–F1073, https://doi.org/10.1149/2.103309jes.
[19] M. Ayoub, et al., Continuous graded catalyst layers for PEM fuel cells with improved humidity range tolerance, J. Electrochem. Soc. 171 (11) (2024) 114503, https://doi.org/10.1149/1945-7111/ad8d81.
[20] S. Li, X. Wei, H. Dai, H. Yuan, P. Ming, Voltammetric and galvanostatic methods for measuring hydrogen crossover in fuel cell, iScience 25 (1) (2022) 103576, https://doi.org/10.1016/j.isci.2021.103576.
[21] J. Zhang, H. Zhang, J. Wu, J. Zhang, Chapter 6 - Hydrogen Crossover, in: J. Zhang, H. Zhang, J. Wu, J. Zhang (Eds.), PEM fuel cell testing and diagnosis, Elsevier, Amsterdam, The Netherlands, Kidlington, Oxford, 2013, pp. 171–185. Available: https://doi.org/10.1016/B978-0-444-53688-4.00006-1.

[22] Mahesh Murphy, Nicholas T. Sisofo Lii, Carol A. Baczkowki, Method and device to improve operation of a fuel cell, WO2006081009A2 (Aug 3) (2006). https://patents.google.com/patent/WO2006081009A2/en?oq=WO2006081009A2.
[23] K.C. Neyerlin, W. Gu, J. Jorne, A. Clark, H.A. Gasteiger, Cathode catalyst utilization for the ORR in a PEMFC, J. Electrochem. Soc. 154 (2) (2007) B279, https://doi.org/10.1149/1.2400626.
[24] Y. Liu, et al., Proton conduction and oxygen reduction kinetics in PEM fuel cell cathodes: effects of ionomer-to-carbon ratio and relative humidity, J. Electrochem. Soc. 156 (8) (2009) B970, https://doi.org/10.1149/1.3143965.
[25] J. Zhang, H. Zhang, J. Wu, J. Zhang (Eds.), PEM fuel cell testing and diagnosis, Elsevier, Amsterdam, The Netherlands, Kidlington, Oxford, 2013.